AIMS Materials Science, 13(3): 474–501.
DOI: 10.3934/matersci.2026023
Received: 12 January 2026
Revised: 29 April 2026
Accepted: 15 May 2026
Published: 28 May 2026

https://www.aimspress.com/journal/Materials

*Research article*

# Effect of $TiO_2$ nanoparticles at low concentrations on PLA and reprocessed PLA nanocomposites properties for 3D printing applications

**Thomas Rodríguez[1], Nacarí Marín-Calvo[1,2], Yessica Sáez[2,3], Simón Faba[4], Marina Patricia Arrieta[4,5] and Edwin Collado[2,3,*]**

[1] Facultad de Ingeniería Mecánica, Universidad Tecnológica de Panamá, Los Santos, Panamá
[2] Centro de Estudios Multidisciplinarios en Ciencias, Ingeniería y Tecnología (CEMCIT AIP), Panamá
[3] Facultad de Ingeniería Eléctrica, Universidad Tecnológica de Panamá, Los Santos, Panamá
[4] Departamento de Ingeniería Química Industrial y del Medio Ambiente, Escuela Técnica Superior de Ingenieros Industriales, Universidad Politécnica de Madrid (ETSII-UPM), C/José Gutiérrez Abascal 2, 28006 Madrid, Spain
[5] Grupo de Investigación: Polímeros, Caracterización y Aplicaciones (POLCA), 28006 Madrid, Spain

* **Correspondence:** Email: edwin.collado@utp.ac.pa.

**Abstract:** Environmental concerns over plastic waste have increased the demand for sustainable materials in additive manufacturing. Polylactic acid (PLA), a biodegradable polymer, is widely used in 3D printing but is limited by poor thermal and ultraviolet (UV) durability. This study explored the development of PLA composite filaments for fused filament fabrication (FFF) by combining virgin PLA (vPLA), reprocessed PLA (rPLA), and titanium dioxide ($TiO_2$) nanoparticles at 0.25 and 0.5 wt.% for 3D-printing material. Six PLA-$TiO_2$-based formulations were melt-extruded into filaments using a single-screw laboratory extruder, with processing adjusted to the $TiO_2$ content to ensure filament quality. The resulting filaments were then used to fabricate 3D-printed specimens for subsequent mechanical, thermal, and structural characterization. Results show that incorporation of $TiO_2$ nanoparticles improves the thermal stability and mechanical performance affected by the recycling process. Fourier transform infrared spectroscopy (FTIR) analysis confirmed chemical integrity, and thermogravimetric analysis (TGA) and tensile testing showed increased stiffness and thermal resistance. Additionally, rPLA accelerates biodegradation in compost due to its reduced structural integrity and increased hydrophilicity, while $TiO_2$ nanoparticles can slightly mitigate this effect in higher concentrations.

**Keywords:** 3D printing; characterization; compostability; FFF; PLA; $TiO_2$

## 1. Introduction

The increasing concern over environmental pollution caused by non-degradable plastic waste has accelerated the transition toward sustainable and biodegradable polymers. Among bioplastics, polylactic acid (PLA) has emerged as a leading candidate to replace petroleum-based polymers due to its biodegradability, compostability, and derivation from renewable sources like corn starch or sugarcane [1–4]. PLA offers several advantages, such as high stiffness, good transparency, and ease of processing, making it suitable for applications in packaging, agriculture, biomedicine, electronics, and 3D printing [5–8]. Following the objectives established for 2030 by the European Commission to introduce recycled plastics in a circular economy and to increase the content of recycled material in all single-use plastic products, PLA has demonstrated its suitability to be recycled, mainly when it comes from a well-known origin, such as industrial production, in which several defective plastic parts and/or plastic burrs are discarded from the production line [9].

Additive manufacturing, particularly fused filament fabrication (FFF), has become a prominent platform for processing PLA. FFF enables layer-by-layer fabrication of complex geometries directly from digital models, with significant advantages in terms of cost-effectiveness, minimal waste generation, and design freedom compared to traditional manufacturing methods, such as injection molding or subtractive machining [10,11]. Due to its relatively low processing temperature and dimensional stability, PLA is widely used as the reference material for desktop FFF [12]. However, PLA still presents inherent limitations such as brittleness, low thermal resistance, and susceptibility to photodegradation, which restrict its performance in technical and outdoor applications [2,13,14]. To mitigate these drawbacks, extensive research has focused on PLA-based composites incorporating natural fibers, nanomaterials, and recycled fractions. Reported strategies include polymer blending, copolymerization, and the incorporation of functional additives or nanofillers to modify mechanical, thermal, and durability properties of PLA [2,3,15]. In this context, titanium dioxide ($TiO_2$) has attracted significant attention due to its multifunctional properties.

$TiO_2$ is chemically stable, inexpensive, and widely used as a photocatalyst, ultraviolet (UV) blocker, and antimicrobial agent in polymeric systems [1,16,17]. It crystallizes mainly in anatase and rutile forms, which are the most relevant for polymer composites and display distinct photocatalytic activity and UV-shielding efficiency [5]. The incorporation of $TiO_2$ into PLA matrices has been reported to improve their thermal stability [11,14], mechanical performance [10], and UV resistance [6,15]. In polymer nanocomposites, the efficiency of nanoparticle reinforcement is strongly influenced by interfacial interactions between the filler surface and the polymer matrix. Metal oxide nanoparticles such as $TiO_2$ typically contain surface hydroxyl groups that can interact with polar functional groups present in PLA, including ester and carbonyl moieties. These interactions can promote physical adsorption at the polymer–particle interface, improving stress transfer efficiency and restricting polymer chain mobility in the vicinity of the nanoparticles. Even in the absence of chemical bonding, such interfacial interactions can significantly influence the mechanical and thermal response of the composite when the nanoparticles are well dispersed within the matrix [1,4,11]. For instance, Antunes et al. reported that PLA-$TiO_2$ nanocomposites exhibited delayed degradation and increased

crystallinity under accelerated weathering conditions [5]. Similarly, Cao et al. achieved improved mechanical strength and excellent UV resistance by using double-shell structured $TiO_2$ nanohybrids in stereocomplex PLA matrices, preventing photocatalytic damage [6]. Additionally, $TiO_2$ nanoparticles can act as nucleating agents, influencing the crystallization kinetics of PLA and improving dimensional stability during thermal cycles [18]. The method of incorporating $TiO_2$, including melt extrusion, solvent casting, or in situ polymerization, significantly affects nanoparticle dispersion and, consequently, composite performance [10]. Recent advances have focused on surface modification of $TiO_2$ particles to enhance compatibility with the hydrophobic PLA matrix and prevent agglomeration [1].

Moreover, studies have shown that $TiO_2$ can compensate for the loss in mechanical performance caused by the inclusion of recycled PLA (RPLA), making PLA-$TiO_2$ composites particularly attractive for circular manufacturing models [10]. In this context, RPLA generally refers to PLA recovered from post-consumer or post-industrial waste streams, while reprocessed PLA (rPLA) refers to PLA that has undergone additional thermal and mechanical processing cycles, such as extrusion or 3D printing, without necessarily originating from external waste sources. The use of rPLA and RPLA aligns with global efforts to reduce the environmental footprint of single-use plastic products and promotes the development of sustainable materials for additive manufacturing [10]. In addition to improving thermal stability and UV resistance, $TiO_2$ nanoparticles have also been reported to act as nucleating agents in PLA matrices, potentially modifying crystallization kinetics and crystalline structure [4,11,18].

Although numerous studies have investigated PLA-$TiO_2$ nanocomposites [5,10,11,14], and others have addressed the mechanical and thermal behavior of RPLA systems [18–21], most reported systems employ relatively high nanoparticle concentrations, typically ranging from 1 to 5 wt.% or even higher [22–25]. Such concentrations often require surface modification of the nanoparticles, compatibilizing agents, or alternative processing techniques to prevent agglomeration and ensure adequate dispersion within the polymer matrix. While these strategies can improve certain properties, they may also increase processing complexity, cost, and potential impacts on recyclability and biodegradability.

Some studies have explored relatively low $TiO_2$ contents in PLA matrices. For example, Zhang et al. reported that $TiO_2$ concentrations around 0.5 wt.% can influence crystallization behavior and enhance the thermal stability of PLA nanocomposites [11]. Other studies evaluating antibacterial or functional PLA/$TiO_2$ systems have used similar ranges (≈0.5–0.75 wt.%), reporting improvements in mechanical and functional properties [23]. Additionally, review studies indicate that low $TiO_2$ loadings may act as nucleating agents, affecting the crystallization behavior of PLA [1]. However, despite these contributions, the literature remains largely focused on virgin PLA systems, with limited studies addressing ultra-low $TiO_2$ concentrations (≤0.5 wt.%) in RPLA. This gap is particularly evident in filament-based additive manufacturing processes such as FFF. Moreover, most existing research emphasizes functional properties (e.g., UV shielding, antibacterial activity, or photocatalysis) rather than the combined effects of ultra-low nanoparticle loading on the thermal, mechanical, and processing behavior of recycled polymer systems. In this context, the potential of ultra-low $TiO_2$ concentrations (≤0.5 wt.%) remains comparatively underexplored, particularly in filament-based additive manufacturing systems. Investigating this low concentration range allows the evaluation of whether minimal nanoparticle additions can produce measurable improvements in thermal and mechanical performance while maintaining good processability, minimizing agglomeration effects, and preserving the environmental advantages of PLA-based materials.

Based on this background, the aim of this study is to evaluate the macroscopic thermal, mechanical, structural, and biodegradation performance of PLA-based composites containing 30 wt.% rPLA, in line with current regulations promoting the incorporation of recycled content in plastics [26–28], and low concentrations of $TiO_2$ nanoparticles (0.25 and 0.5 wt.%), processed via filament extrusion for FFF 3D-printing applications. The central hypothesis is that $TiO_2$ can act as a multifunctional additive capable of partially mitigating the degradation effects associated with rPLA without compromising processability or printability. To assess these effects, the study focuses on macroscopic characterization techniques, including Fourier transform infrared spectroscopy (FTIR) analysis, thermogravimetric analysis (TGA), tensile testing, wettability analysis, and composting behavior. Additionally, operating within this low nanoparticle concentration range allows the evaluation of reinforcement mechanisms without the use of compatibilizers or surface-modified nanoparticles, thereby preserving a simple and scalable processing route compatible with FFF technologies and contributing to the development of more sustainable filament materials for additive manufacturing applications, such as functional prototypes, electronic housings, and other non-structural components.

## 2. Materials and methods

### *2.1. Materials*

PLA, Ingeo™ Biopolymer 2003D, is commercialized in pellet form by NatureWorks LLC (Minnetonka, MN, USA) [29]. This PLA grade has a melt flow rate (MFR) at 210 ºC of 6 g/10 min and a true density of 1.24 $g \cdot cm^{-3}$. Titania nanotubes powder (CAS 13463-67-7) was provided by Sigma-Aldrich S.A. (Madrid, Spain). According to specifications [30], $TiO_2$ density is 4.26 $g \cdot cm^{-3}$, while nanotube diameters are 25 nm, with a length of 1–5 μm, an effective surface area of 150–200 $m^2 \cdot g^{-1}$, and a pore volume of 0.2–0.6 $cm^3 \cdot g^{-1}$.

### *2.2. Simulation of rPLA*

The rPLA used in this study was reprocessed to simulate the recovery of PLA defective parts produced at the industrial level based on the procedure described by Sepulveda et al. [9]. Initially, virgin PLA (vPLA) pellets were extruded into filament using a Composer 350 filament maker (3DEVO, Netherlands) single-screw filament extruder under the machine PLA default processing profile for PLA filament at 1.75 mm diameter, with temperature zones set at 170, 185, 190, and 170 ºC from hopper to die, corresponding to the four heating zones of the extrusion system (see Figure 1), and a screw speed of 3.5 $min^{-1}$. This filament was then mechanically pelletized into short segments (approximately 2–4 mm in length) to simulate post-use waste. The resulting rPLA pellets were subsequently reprocessed following the same drying and extrusion protocols applied to the virgin material, ensuring consistency in the formulation and processing history.

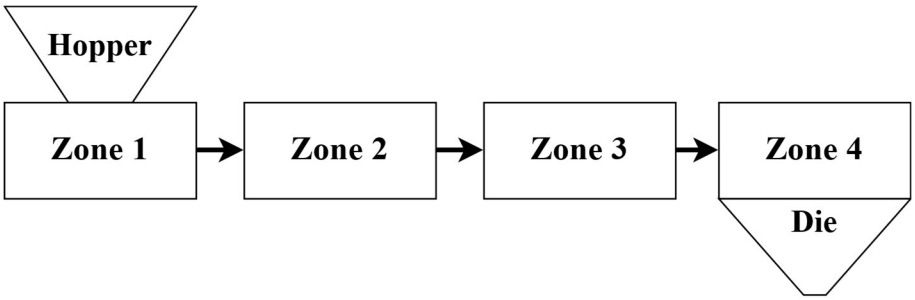


**Figure 1.** Representative diagram of heating zones from the filament extruder.

*2.3. PLA, rPLA, and $TiO_2$ formulations and processing*

In this study, six different material formulations were prepared to evaluate the effects of incorporating $TiO_2$ nanoparticles into vPLA and rPLA matrices. The formulations include pure PLA, PLA containing 30 wt.% of rPLA (PLA-rPLA), PLA loaded with different weight percentages of $TiO_2$ (0.25 and 0.50 wt.%), and two additional samples combining both rPLA and $TiO_2$ at the same loading levels. The composition of the formulations is detailed in Table 1.

**Table 1.** Summary of the study formulations.

| Material | vPLA (wt.%) | rPLA (wt.%) | $TiO_2$ (wt.%) |
|---|---|---|---|
| PLA | 100.000 | 0.000 | 0.000 |
| PLA-0.25$TiO_2$ | 99.750 | 0.000 | 0.250 |
| PLA-0.5$TiO_2$ | 99.500 | 0.000 | 0.500 |
| PLA-rPLA | 70.000 | 30.000 | 0.000 |
| PLA-rPLA-0.25$TiO_2$ | 69.825 | 29.925 | 0.250 |
| PLA-rPLA-0.5$TiO_2$ | 69.650 | 29.850 | 0.500 |

It is important to note that during the complete processing route, the polymer experiences multiple thermal cycles. In the present experimental design, the rPLA fraction was intentionally subjected to an additional extrusion step prior to formulation preparation in order to simulate mechanically RPLA originating from industrial filament production waste. After this simulated recycling step, all formulations, including neat PLA, PLA-$TiO_2$, PLA-rPLA, and PLA-rPLA-$TiO_2$, were processed under identical conditions during filament extrusion and subsequent FFF printing. Therefore, the rPLA fraction experienced one additional thermo-mechanical processing cycle compared to the virgin PLA fraction, allowing the study to reproduce the structural changes associated with RPLA while maintaining comparable processing histories across all formulations.

The selected formulations were designed to evaluate the individual and combined effects of $TiO_2$ nanoparticles and rPLA content under conventional processing conditions. $TiO_2$ loadings of 0.25 and 0.50 wt.% were selected to maintain the filler concentration low, thereby minimizing agglomeration and favoring dispersion in the PLA matrix during extrusion, without using compatibilizers, surfactants, or other dispersion aids. These concentrations also fall within the range commonly reported to improve thermal stability and UV resistance without compromising

processability [6,11,31]. Operating within this low concentration range also enables the assessment of reinforcement mechanisms without the use of compatibilizers or surface-modified nanoparticles, thereby maintaining a simple and scalable processing route compatible with FFF technologies. A rPLA content of 30 wt.% was selected as an industrially relevant level that enables substantial material recovery while maintaining acceptable mechanical performance. This compositional approach allows direct comparison between virgin and reprocessed matrices and the assessment of potential synergistic effects between $TiO_2$ addition and reprocessed content. It also reflects the dispersion achievable under the selected processing conditions.

A comprehensive diagram of the compositional process is presented in Figure 2. Prior to processing, all materials including vPLA, rPLA, and $TiO_2$ were dried in a Q0-F oven (J.P. SELECTA, Spain) at 80 ºC for at least 24 h to minimize moisture-related degradation during extrusion. The formulations were prepared by mixing the specified proportions of each component, previously weighed using a Sartorius Secura SECURA26-1S microanalytical balance (Sartorius, Germany). Filament production was carried out using the methodology described in section 2.2. The target diameter for the filaments was 1.70 ± 0.20 mm. Filament diameter was monitored continuously during extrusion and verified post-extrusion using digital calipers. Two extrusion profiles were applied depending on the formulation. For PLA and PLA-rPLA blends, the temperature zones and screw speed used were described at section 2.2. For PLA-$TiO_2$ and PLA-rPLA-$TiO_2$ formulations, the temperature profile was adjusted at 170, 185, 190, and 180 ºC, with a screw speed of 4.0 $min^{-1}$ to improve filament diameter stability. Test specimens were fabricated using the obtained filaments on a Creality K2 Plus 3D printer (Creality, Shenzhen, China) with a 0.4 mm nozzle diameter, employing FFF technology (Figure 2).

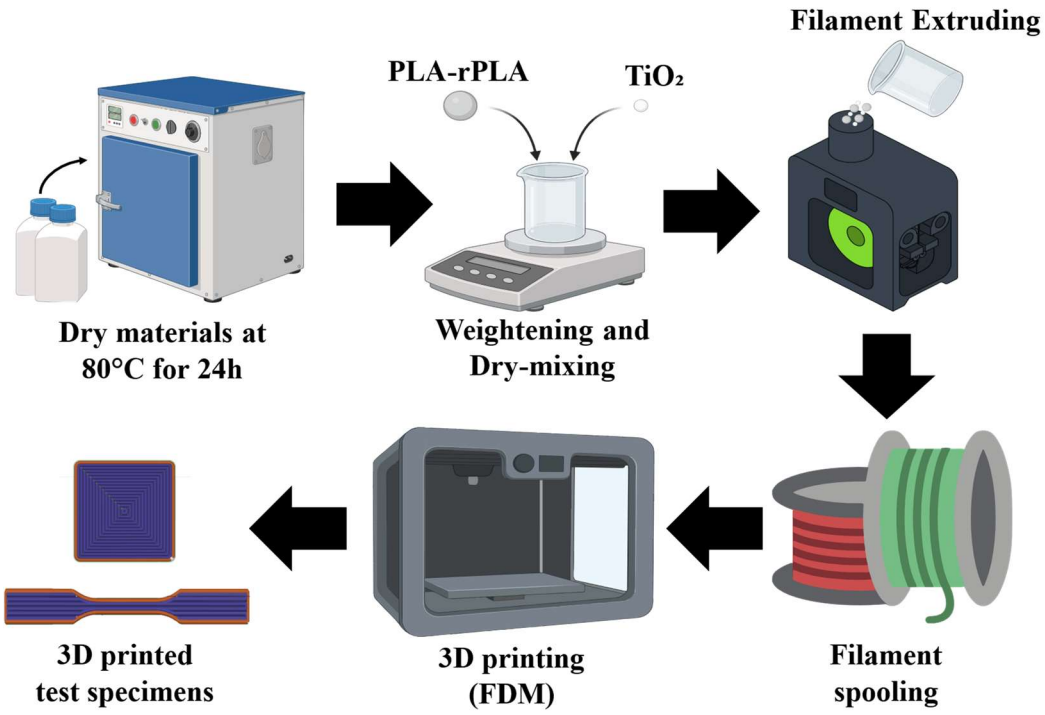


**Figure 2.** Schematic representation of the fabrication process for 3D-printing specimens.

The printing parameters were set as follows: a nozzle temperature of 220 ºC, bed temperature of 65 ºC, printing speed of 50 mm/s, layer height of 0.2 mm, and 100% infill density were used for all samples to ensure consistent material deposition and minimize internal porosity. Both tensile and composting specimens were intentionally printed as single-layer structures with a nominal thickness of 0.2 mm. This approach was selected to minimize the influence of interlayer adhesion and to ensure that the evaluated properties primarily reflect the intrinsic material behavior rather than interlayer bonding effects. Due to the single-layer configuration and 100% infill, no additional shell layers or top/bottom layers were required. Tensile specimens were printed with raster lines oriented parallel to the loading direction (0° raster angle) to reduce anisotropic effects and ensure that mechanical testing primarily reflects material behavior rather than interlayer adhesion limitations. The infill pattern for tensile specimens was rectilinear, with no additional shell layers to maintain uniform cross-sections. Composting specimens were printed using a concentric infill pattern. The printing orientation was maintained in the XY plane for all samples, with the build direction corresponding to the Z-axis. The dimensional accuracy of each specimen was verified prior to characterization to ensure consistency and reliability of the printed samples.

### *2.4. Spectroscopic characterization*

Attenuated total reflectance Fourier transform infrared (ATR-FTIR) spectroscopy was employed to analyze the principal functional groups of PLA nanocomposite specimens. The analysis was run at ambient temperature in transmission mode in an FT/IR-4X infrared spectrometer (JASCO Inc., Tokyo, Japan). The procedure followed the guidelines of ASTM E1252, which provides general practices for acquiring infrared spectra [32]. The experimental wavenumber range was within 4000–400 $cm^{-1}$, the resolution was 4 $cm^{-1}$, and 64 scans were performed. The ranges used were selected according to the operational capabilities of the equipment. Squared specimens were used for these tests.

### *2.5. Thermal properties*

TGA was used to determine the type of degradation and to evaluate the thermal stability of the specimens developed in this work. The experiments were done in a SETARAM TGA analyzer (SETARAM, Caluire, France) from 40 to 800 ºC at a heating rate of 10 $ºC \cdot min^{-1}$ under a nitrogen atmosphere (gas flow of 30 $mL \cdot min^{-1}$) [26]. Fragments of dog-bone specimens from approximately 6–10 mg were used for these tests.

### *2.6. Mechanical properties*

Mechanical properties were evaluated by means of tensile test measurements using a Shimadzu AGS-X 100 N universal tensile testing machine (Shimadzu Corpo-194 ration, Kyoto, Japan) equipped with a 100 N load cell, with an initial length of 20 mm and a crosshead speed of 10 $mm \cdot min^{-1}$. Dog-bone samples, as seen in Figure 3, were prepared by an FFF 3D printer Creality K2 Plus (Creality, Shenzhen, China) for tensile specimen 1BB, according to ISO 527-2 [33]. Mechanical testing was performed using 10 specimens per formulation; the reported values correspond to the mean ± standard deviation. The Young's modulus ($E$), tensile strength ($\sigma$), and elongation at break ($\varepsilon\%$) were determined from the corresponding stress–strain curves. $E$ was determined from the initial linear elastic

region of the stress–strain curve. A linear regression was applied within the strain range corresponding to the elastic deformation region, and the slope of this linear fit was reported as the modulus.

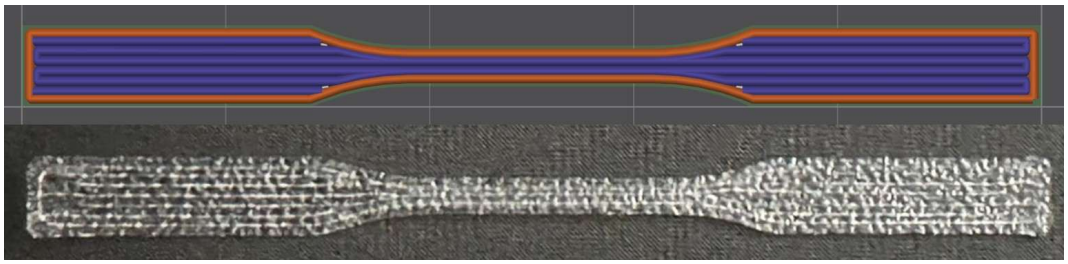

**Figure 3.** Tensile specimen prepared for FFF printing.

*2.7. Degradation under composting conditions*

The specimens were disintegrated under laboratory-scale composting conditions, in accordance with ISO 20200 standards [34]. Samples, 3D printed into 15 × 15 mm squares (Figure 4), were placed inside textile mesh and buried in perforated plastic boxes filled with prepared compost soil. The textile mesh enabled direct contact with the compost while facilitating the retrieval of degraded material, according to the procedure of Arrieta et al. [35]. The composting mixture was composed of approximately 40% sawdust, 30% rabbit feed, 10% compost, 10% corn starch, 5% sugar, 4% corn oil, and 1% urea. Deionized water was added until the mixture reached 55 wt.% of water content. The boxes were maintained under aerobic conditions at 58 ºC. Samples were excavated after 1, 4, 7, 16, 23, and 28 days, subsequently dried in an oven at 40 ºC for 24 h, and then weighed and photographed for visual comparison.

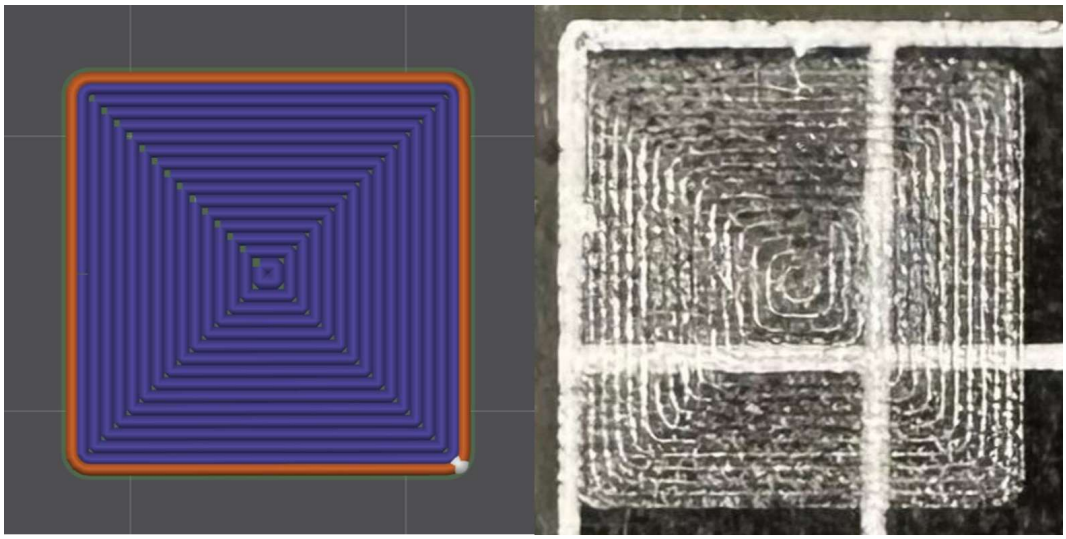

**Figure 4.** Composting specimen prepared for FFF printing.

### *2.8. Water contact angle (WCA)*

Contact angle measurements were performed using an Ossila Contact Angle Goniometer (Ossila Ltd., The Netherlands), equipped with a video capture system and analysis software (Contact Angle Release Notes-4.2.2). The WCA followed the UNE: EN ISO 828:2013 standard [36] by randomly adding at least five drops of distilled water (10 μL) with a syringe to the specimens' surfaces at room temperature and measuring the contact angle after 10 s of water drop deposition. Squared specimens with increased thickness (1 mm) were used for these tests.

### *2.9. Statistical analysis*

Statistical analysis was performed using one-way ANOVA to evaluate the significance of differences among the six material formulations. The analysis was conducted for Young's modulus, tensile strength, elongation at break, and water contact angle measurements using a significance level of $\alpha = 0.05$, which is a threshold that defines the maximum acceptable probability of making a Type I error in a hypothesis test. When significant differences were detected, Tukey's post hoc multiple comparison test was applied to identify statistically distinct groups among the formulations. Effect sizes were evaluated using eta-squared ($\eta^2$) and Cohen's f statistics to quantify the magnitude of differences between groups.

In the ANOVA analysis, the F value represents the ratio between the variance among group means and the variance within groups, with higher F values indicating greater differences among formulations. The *p-value* indicates the probability of obtaining the observed differences assuming that no real differences exist among groups. Statistical significance was determined using a significance level of $\alpha = 0.05$; therefore, results with $p < 0.05$ were considered statistically significant. The effect size was quantified using $\eta^2$, which represents the proportion of total variance explained by the grouping factor, where larger $\eta^2$ values indicate a stronger effect of formulation on the measured property. Cohen's f was also calculated as a standardized measure of effect size for ANOVA, with values of 0.10, 0.25, and 0.40 commonly interpreted as small, medium, and large effects, respectively. For Tukey's post hoc multiple comparison test, different letters (*a*, *b*, and *c*) assigned to the samples in the graphs indicate statistically significant differences between groups ($p < 0.05$), whereas groups sharing the same letter are not significantly different from each other.

## 3. Results and discussion

### *3.1. 3D-printed specimens*

Figure 5 shows visual differences among the printed specimens despite all samples being manufactured as single-layer structures with a nominal thickness of 0.2 mm. The tensile specimens, printed with raster lines parallel to the loading direction, exhibit adequate filament definition and edge sharpness from neat PLA to $TiO_2$-filled formulations, while rPLA-containing samples show less uniform line width and locally rougher surfaces. PLA-rPLA specimens display irregular filament deposition and slight thinning in the gauge section, indicating less stable melt flow. For the composting specimens printed with a concentric pattern, neat PLA and PLA-$TiO_2$ samples show well-defined and

continuous concentric paths, whereas rPLA-based specimens present noticeable defects such as incomplete bonding between adjacent rasters, gaps, and increased surface heterogeneity.

The printing irregularities observed in rPLA-containing samples can be attributed to rheological changes resulting from molecular weight reduction during PLA reprocessing. Thermo-mechanical processing of PLA is known to induce chain scission, resulting in a reduction in molecular weight and melt viscosity [24,25]. Lower-molecular-weight polymers generally exhibit reduced melt viscosity and altered flow behavior during extrusion, which can affect filament diameter stability and deposition accuracy during FFF. Variations in filament deposition and interlayer bonding may therefore contribute to the mechanical response of printed specimens, particularly in terms of ductility and stress distribution [37]. Similar relationships between polymer degradation, melt viscosity, and printing quality have been reported in previous studies on RPLA materials [10].

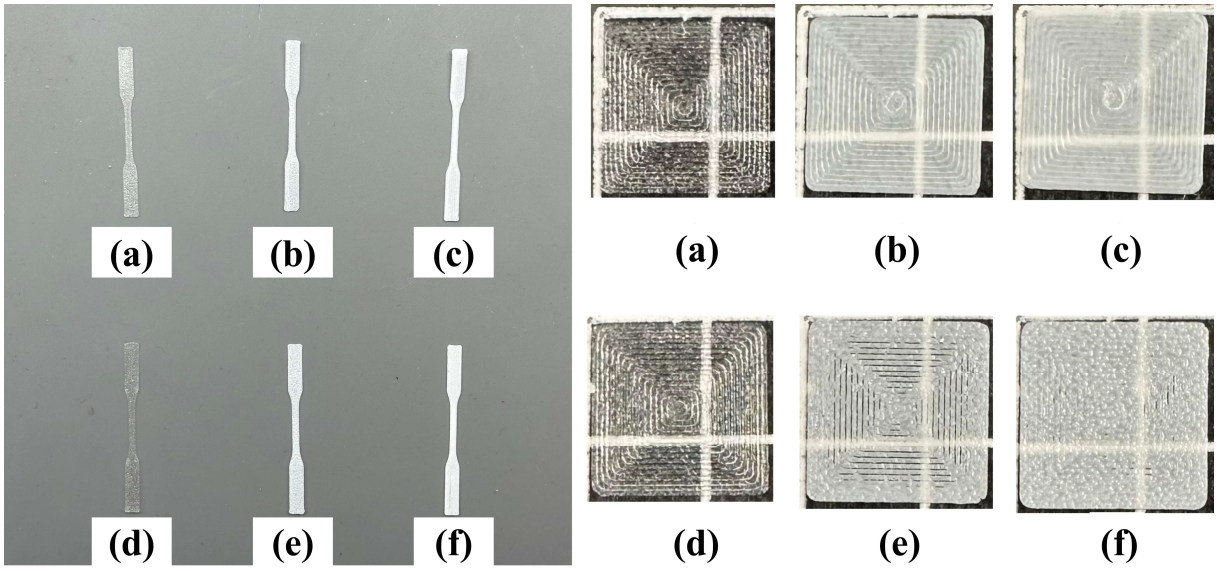


**Figure 5.** Tensile specimens (left) and composting specimens (right) prepared with FFF printing from: (a) PLA, (b) PLA-0.25$TiO_2$, (c) PLA-0.50$TiO_2$, (d) PLA-rPLA, (e) PLA-rPLA-0.25$TiO_2$, and (f) PLA-rPLA-0.50$TiO_2$.

*3.2. Spectroscopic characterization*

FTIR was employed to analyze the characteristic functional groups of PLA-based and corresponding nanocomposite specimens. The spectra of the different formulations are presented in Figure 6. The spectra are vertically offset for clarity, enabling direct comparison across different formulations. In all samples, the characteristic absorption bands of PLA are observed, confirming that the base polymeric structure remains largely preserved after blending and nanoparticle incorporation. The absorption band at ~1745 $cm^{-1}$ corresponds to the stretching vibration of the carbonyl group (C=O), which is the most prominent functional group in PLA. The position, shape, and relative intensity of this band remain essentially identical for all formulations, suggesting preservation of the ester linkages and the absence of significant chain scission or chemical degradation. Similarly, the absorption bands between 1180 and 1080 $cm^{-1}$ are attributed to C–O–C stretching vibrations of the ester linkage, reinforcing the identification of the polyester backbone [38,39].

The band located at ~1450 $cm^{-1}$ corresponds to $CH_3$ bending vibrations, while weak absorptions at ~2995 and 2945 $cm^{-1}$ are assigned to aliphatic C–H stretching. These assignments are consistent with previous reports for neat PLA [19,21] and show no meaningful shifts or intensity variations across the different formulations, indicating that neither thermal processing nor the addition of rPLA and $TiO_2$ induce detectable chemical modifications in the PLA structure. In the low wavenumber region (400–800 $cm^{-1}$), a weak absorption contribution is observed in the $TiO_2$-containing samples, which can be associated with Ti–O vibrational modes [15,19–22,40]. However, this contribution is subtle and does not significantly affect the overall spectral profile. Importantly, no new absorption bands, peak splitting, or systematic band shifts are detected in this region or elsewhere in the spectra. FTIR results demonstrate that all formulations retain the characteristic chemical signature of PLA. The incorporation of rPLA and low $TiO_2$ loadings (0.25–0.5 wt.%) does not lead to the formation of new functional groups or measurable chemical interactions detectable by FTIR.

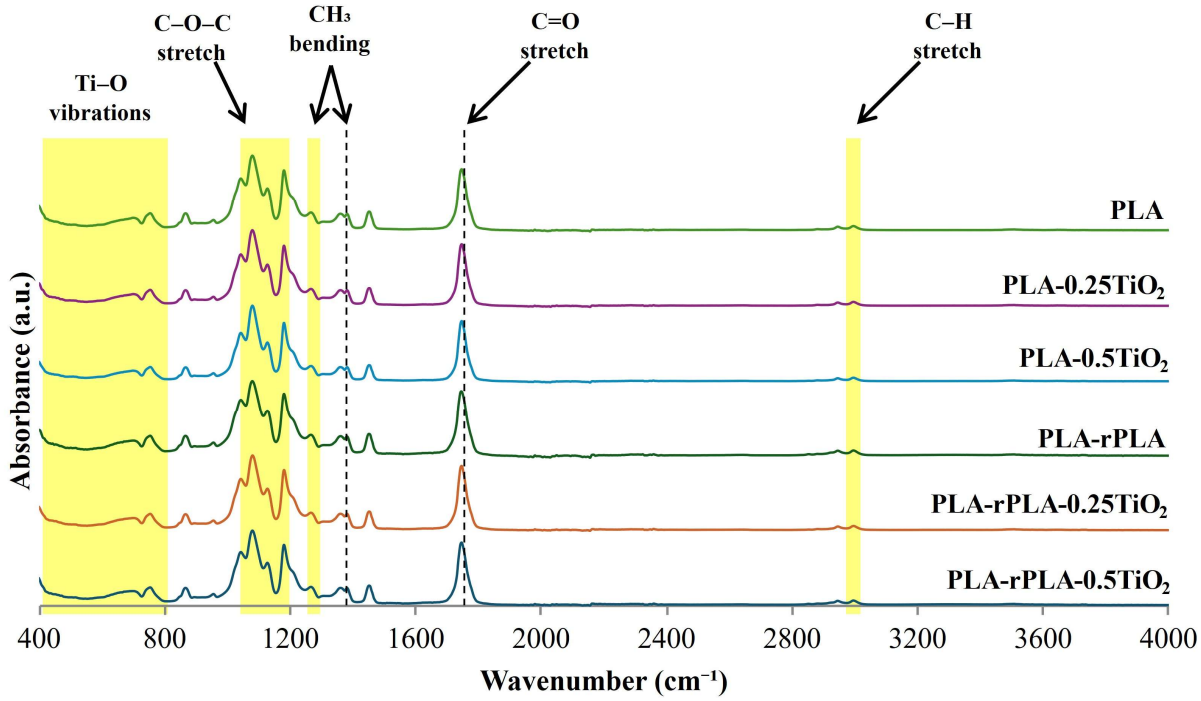


**Figure 6.** FTIR-ATR spectra of PLA, rPLA, and PLA-$TiO_2$ samples.

### *3.3. Thermal characterization*

A thermal characterization was carried out to determine the effect of reprocessed content and nanoparticle incorporation on the onset of thermal degradation and on the overall resistance of the materials to thermal decomposition. TGA was performed to evaluate the thermal stability and degradation behavior of neat PLA, PLA reinforced with $TiO_2$ nanoparticles (0.25 and 0.50 wt.%), PLA-rPLA, and PLA-$TiO_2$ nanocomposite 3D parts. Figure 7 shows the TGA and derivative thermogravimetric (DTG) curves for the studied formulations, while Table 2 summarizes the main thermal parameters, including the temperature at 5% weight loss ($T_{d,5\%}$) as the onset temperature and maximum degradation temperature ($T_{max}$). These parameters are widely recognized as reliable indicators of thermal stability in polymeric systems [10,19,41].

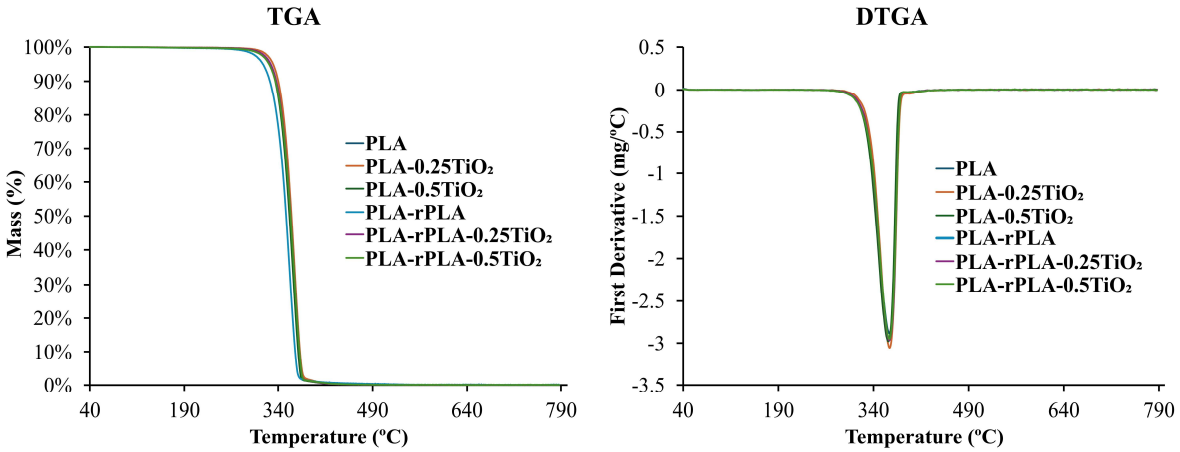


**Figure 7.** TGA and DTGA curves of PLA, rPLA, and PLA-$TiO_2$ composite specimens.

**Table 2.** TGA parameters of the PLA, rPLA, and PLA-$TiO_2$ composite specimens.

| Material | $T_{d,5\%}$ (°C) | $T_{max}$ (°C) | Residual mass (%) |
|---|---|---|---|
| PLA | 326.8 | 365.3 | 0.02 |
| PLA-0.25$TiO_2$ | 331.4 | 365.7 | 0.05 |
| PLA-0.5$TiO_2$ | 326.2 | 363.7 | 0.07 |
| PLA-rPLA | 315.2 | 357.7 | 0.10 |
| PLA-rPLA-0.25$TiO_2$ | 327.6 | 365.0 | 0.01 |
| PLA-rPLA-0.5$TiO_2$ | 324.9 | 365.3 | 0.06 |

All materials exhibited a single main degradation step between 300 and 380 °C, consistent with the decomposition of the PLA backbone and characteristic of PLA-based thermoplastics [9]. Neat PLA showed a $T_{d,5\%}$ of 326.8 °C and a $T_{max}$ of 365.3 °C. The addition of $TiO_2$ nanoparticles led to a moderate improvement in thermal stability, particularly with PLA-0.25$TiO_2$ reaching a $T_{d,5\%}$ of 331.4 °C and a $T_{max}$ of 365.7 °C. At a higher $TiO_2$ loading (0.5 wt.%), $T_{d,5\%}$ decreased slightly to 326.2 °C, while $T_{max}$ remained elevated at 363.7 °C. Interestingly, the improvement in thermal stability was more pronounced at the lower $TiO_2$ loading (0.25 wt.%) compared to the higher concentration (0.5 wt.%). This behavior has been frequently reported in polymer nanocomposites and is generally associated with dispersion effects and nanoparticle interactions within the polymer matrix [1,4,18]. At very low nanoparticle concentrations, $TiO_2$ particles can be more uniformly distributed within the polymer matrix, creating an effective barrier that limits heat transfer and the diffusion of volatile degradation products during thermal decomposition [18,40]. However, as the nanoparticle concentration increases, the probability of particle agglomeration also increases due to the high surface energy of $TiO_2$ nanoparticles. Such agglomerates can act as localized defects within the polymer matrix, reducing the effectiveness of the barrier effect and potentially facilitating thermal degradation pathways [1,4]. Therefore, the slightly lower $T_{d,5\%}$ observed for the 0.5 wt.% $TiO_2$ formulation may reflect the onset of nanoparticle clustering and less efficient dispersion under the selected melt processing conditions. However, this interpretation is based on trends reported in the literature, and additional experimental characterization would be required to confirm the presence of nanoparticle aggregation in the present system.

On the other hand, PLA-rPLA blend displayed a reduction in thermal stability, with $T_{d,5\%}$ decreasing to 315.2 ºC and $T_{max}$ to 357.7 ºC. This behavior is attributed to chain scission and molecular weight reduction associated with previous thermal and mechanical processing of the rPLA fraction [9,10]. Despite this reduction, the addition of $TiO_2$ to the PLA-rPLA matrix partially restored thermal stability. PLA-rPLA-0.25 $TiO_2$ and PLA-rPLA-0.5 $TiO_2$ exhibited $T_{d,5\%}$ values of 327.6 and 324.9 ºC, respectively, while $T_{max}$ values converged around ~365 ºC, comparable to those of neat PLA and PLA-$TiO_2$ systems. Previous investigations on mechanically rPLA under similar processing conditions have consistently reported reductions in number-average and weight-average molecular weight due to thermo-mechanical degradation [24,25,42]. The reduced thermal stability observed in PLA-rPLA systems is consistent with the additional thermo-mechanical processing involved in the simulated recycling step, which promotes chain scission and molecular weight reduction in PLA. These phenomena have been widely documented for PLA materials subjected to multiple extrusion cycles [24,42]. Residual mass at 600 ºC was negligible for all formulations (<0.1% for all formulations), confirming the complete decomposition of the PLA matrix and the absence of significant inorganic residue beyond the low $TiO_2$ loadings used. The DTG curves further supported these findings, showing that neat PLA and PLA-rPLA reached maximum degradation rates at lower temperatures, whereas $TiO_2$-containing formulations exhibited a shift of the degradation peak toward higher temperatures, up to approximately 365 ºC. Results confirm that low concentrations of $TiO_2$ can effectively enhance the thermal resistance of PLA-based composites, even in the presence of reprocessed content.

In addition to the barrier effect associated with $TiO_2$ nanoparticles, changes in the crystallization behavior of PLA could also influence the thermal and mechanical performance of printed materials. Thermal processing during filament extrusion and subsequent FFF printing can alter the crystalline fraction of PLA due to differences in cooling rate and thermal history [42,43]. Nanoparticles such as $TiO_2$ can act as nucleating agents within the PLA matrix, potentially modifying crystallization kinetics, crystal size distribution, and overall crystallinity during cooling [4,18]. Variations in crystallinity can significantly affect material properties: increased crystallinity generally enhances stiffness and thermal resistance by stabilizing the polymer structure, whereas lower crystallinity may increase ductility and accelerate degradation processes [42]. Although differential scanning calorimetry (DSC) analysis was not performed in the present study, previous investigations have reported that $TiO_2$ nanoparticles can influence PLA crystallization behavior [4,18]. Therefore, part of the thermal and mechanical behavior observed may also be associated with crystallinity variations induced by both nanoparticle incorporation and the processing history of the material.

### *3.4. Mechanical properties*

The mechanical behavior of the developed formulations was evaluated to obtain a comprehensive understanding of the stiffness, strength, and ductility of the materials, crucial indicators of their suitability for structural applications and additive manufacturing performance. Figure 8 illustrates representative stress–strain curves obtained from tensile testing, Figure 9 shows the mechanical results, and Table 3 summarizes the average values with standard deviations. Neat PLA exhibited a Young's modulus of 1044 ± 46 MPa, a tensile strength of 34.9 ± 0.6 MPa, and an elongation at break of 6.4 ± 0.4%, which is consistent with values commonly reported for FFF-processed PLA [37,44,45]. The incorporation of $TiO_2$ nanoparticles resulted in a clear stiffening effect. The Young's modulus increased to 1102 ± 51 MPa for PLA-0.25 $TiO_2$ and 1159 ± 104 MPa for PLA-0.5$TiO_2$. The increase

in stiffness is consistent with the presence of rigid inorganic particles within the polymer matrix, which can restrict polymer chain mobility and act as reinforcing inclusions, as widely reported in PLA-$TiO_2$ nanocomposites [4,11,18,46]. This stiffening was accompanied by a progressive reduction in ductility, with elongation at break decreasing to 5.6% ± 0.2% and 4.8% ± 0.5%, respectively. In contrast, tensile strength remained largely unchanged for the 0.25 wt.% formulation and increased slightly to 36.0 ± 1.3 MPa at 0.5 wt.% $TiO_2$, indicating that reinforcement did not compromise the load-bearing capacity of the material.

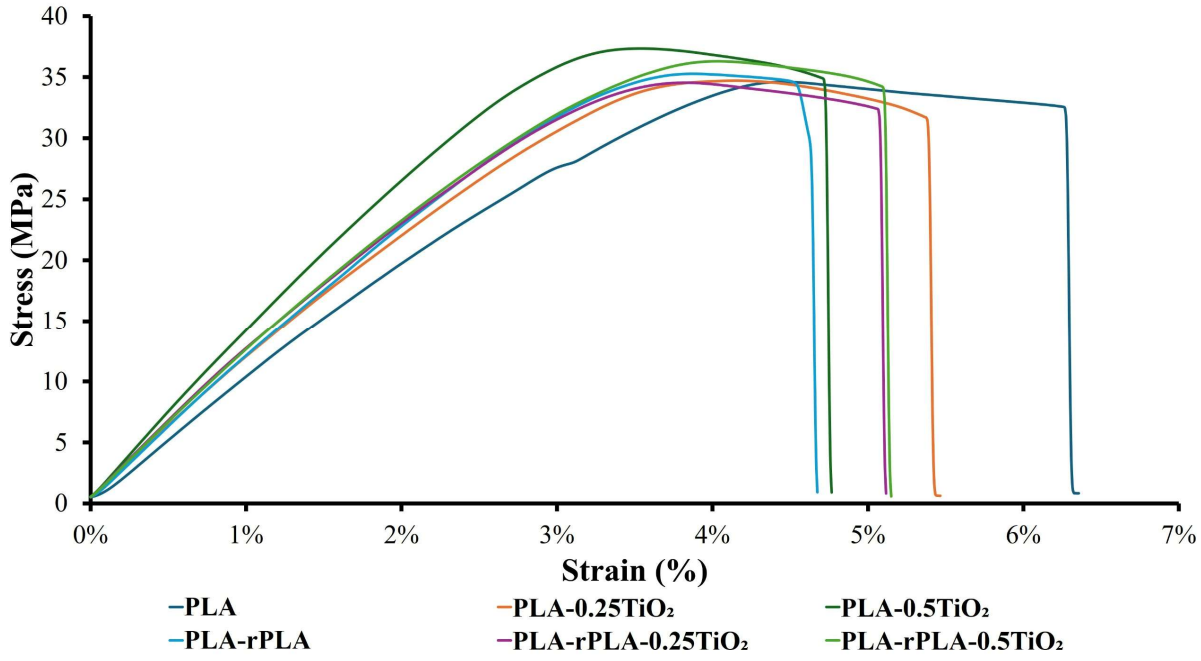


**Figure 8.** Representative stress–strain curves obtained from tensile testing for PLA, rPLA, and $TiO_2$ composites.

The PLA-rPLA blend showed a modest increase in stiffness compared to neat PLA, with a Young's modulus of 1063 ± 35 MPa, while tensile strength remained comparable at 35.4 ± 1.1 MPa. However, elongation at break decreased to 4.8% ± 0.3%, reflecting reduced ductility commonly associated with RPLA due to chain scission and molecular weight reduction during prior processing cycles [9,10]. When $TiO_2$ was incorporated into the PLA-rPLA matrix, a cumulative stiffening effect was observed. PLA-rPLA-0.25$TiO_2$ and PLA-rPLA-0.5$TiO_2$ reached Young's modulus values of 1250 ± 43 and 1288 ± 100 MPa, respectively, representing the highest stiffness among all formulations and an increase of more than 20% relative to neat PLA. The continuous increase in Young's modulus with increasing $TiO_2$ content suggests that even if partial nanoparticle agglomeration occurs at higher loadings, the rigid inorganic phase still contributes to restricting polymer chain mobility, resulting in increased stiffness of the composite material. Similar behavior has been widely reported for polymer nanocomposites, where the incorporation of rigid inorganic nanoparticles increases the elastic modulus of the matrix even when dispersion is not fully ideal [4,11,47].

Tensile strength remained stable or slightly increased (35.7–36.6 MPa), while elongation at break was maintained at approximately 5%, showing a slight recovery compared to the unfilled PLA-rPLA blend. This suggests that $TiO_2$ may partially offset the ductility loss associated with rPLA by improving

stress transfer within the composite. The observed stiffness-ductility trade-off is consistent with previous studies on PLA-$TiO_2$ systems. Similar trends were reported by Zhang et al. [11], who observed increased Young's modulus and reduced elongation at break with increasing $TiO_2$ content, indicating a transition toward a stiffer and more brittle mechanical response. Antunes et al. [5] also reported reduced ductility in PLA-$TiO_2$ composites, which they attributed to nanofiller-induced constraints on PLA chain mobility.

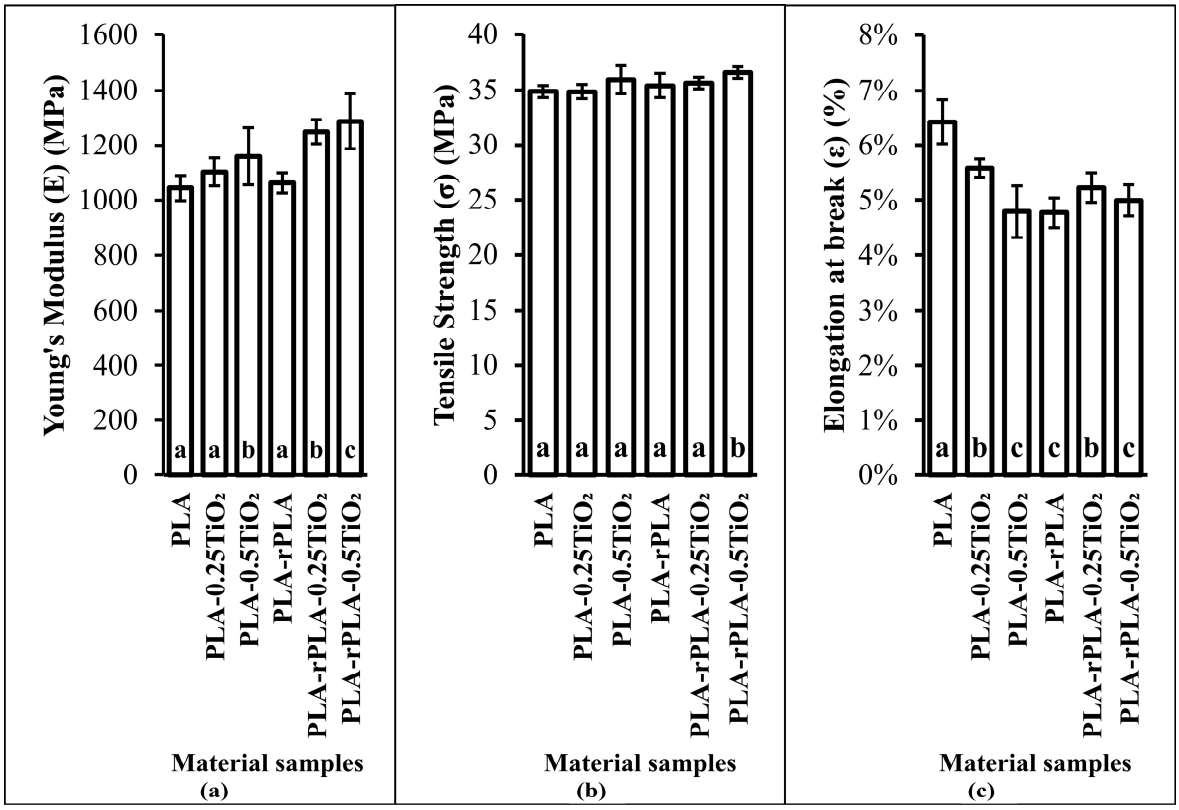


**Figure 9.** (a) Young's modulus, (b) tensile strength, and (c) elongation at break of PLA, rPLA, and PLA-$TiO_2$ composites. Values with different letters are significantly different at $p < 0.05$.

**Table 3.** Mechanical properties of PLA, rPLA, and $TiO_2$ composites.

| Material | Young's modulus (E) (MPa) | Tensile strength (σ) (MPa) | Elongation at break (ε) (%) |
|---|---|---|---|
| PLA | 1044 ± 46 [a] | 34.9 ± 0.6 [a] | 6.4 ± 0.4 [a] |
| PLA-0.25$TiO_2$ | 1102 ± 51 [a] | 34.9 ± 0.7 [a] | 5.6 ± 0.2 [b] |
| PLA-0.5$TiO_2$ | 1159 ± 104 [b] | 36.0 ± 1.3 [a] | 4.8 ± 0.5 [c] |
| PLA-rPLA | 1063 ± 35 [a] | 35.4 ± 1.1 [a] | 4.8 ± 0.3 [c] |
| PLA-rPLA-0.25$TiO_2$ | 1250 ± 43 [b] | 35.7 ± 0.5 [a] | 5.2 ± 0.3 [b] |
| PLA-rPLA-0.5$TiO_2$ | 1288 ± 100 [c] | 36.6 ± 0.5 [b] | 5.0 ± 0.3 [c] |

Values with different letters are significantly different at $p < 0.05$.

The ANOVA analysis revealed significant differences among the formulations for all evaluated properties. Young's modulus showed a strong statistical effect ($F = 20.81$, $p = 1.58 \times 10^{-11}$ indicating that $TiO_2$ incorporation and the presence of rPLA significantly influence the stiffness of the material. Tensile strength also exhibited significant differences ($F = 6.50$, $p = 8.52 \times 10^{-5}$), although with a lower effect size compared to stiffness. Elongation at break presented the strongest statistical effect ($F = 37.70$, $p = 1.92 \times 10^{-16}$), suggesting that ductility is the mechanical property most strongly affected by formulation changes.

The statistical grouping obtained from Tukey's post hoc test (Figure 9) confirms that $TiO_2$-containing formulations form statistically distinct groups with respect to Young's modulus, particularly in the PLA-rPLA-$TiO_2$ systems, which exhibited the highest stiffness values. In contrast, tensile strength differences among several formulations were less pronounced, reflecting the moderate statistical effect observed in the ANOVA analysis. Similarly, elongation at break showed clearly separated statistical groups, confirming the strong influence of both reprocessed content and $TiO_2$ addition on the ductility of the materials.

The reinforcement effect observed in the $TiO_2$-containing formulations is consistent with the behavior commonly reported for polymer nanocomposites, in which rigid inorganic particles act as stress-transfer sites within the polymer matrix [18,47]. At low nanoparticle concentrations, improved particle distribution within the matrix can enhance load transfer efficiency and restrict chain mobility, resulting in increased stiffness [4]. However, the effectiveness of this mechanism strongly depends on nanoparticle dispersion and the quality of the polymer–filler interface. Although direct microstructural characterization using scanning electron microscopy (SEM) or transmission electron microscopy (TEM) was not performed in this study, the mechanical and thermal trends observed are consistent with previously reported PLA-$TiO_2$ systems, where relatively low nanoparticle concentrations produced measurable reinforcement effects [4,18].

### *3.5. Water contact angle*

WCA measurements were performed to evaluate the surface wettability of neat PLA, PLA-$TiO_2$ composites, PLA-rPLA blends, and PLA-rPLA-$TiO_2$ formulations. This parameter provides insight into the hydrophilic or hydrophobic character of the surface, which directly affects moisture absorption, degradation kinetics, and interfacial interactions in composite systems. Figure 10 shows the experimental results, and Table 4 summarizes the mean values.

Neat PLA presented a mean contact angle of 83º ± 3º, confirming its moderately hydrophobic surface behavior and in agreement with previously reported values for PLA-based materials [48–50]. The incorporation of 30 wt.% rPLA significantly reduced the water contact angle to 77º ± 5º, indicating an increase in surface hydrophilicity. This behavior is commonly associated with chain scission and mild oxidative processes during reprocessing, which promote the exposure of polar functional groups such as hydroxyl and carboxyl moieties at the surface, thereby enhancing water affinity [24,25,51]. This increase in hydrophilicity is consistent with the faster biodegradation observed for rPLA-containing systems under composting conditions (section 3.6). The addition of $TiO_2$ nanoparticles resulted in modest, concentration-dependent changes in surface wettability. For neat PLA, incorporation of 0.25 wt.% $TiO_2$ decreased the contact angle to 78º ± 5º, suggesting a slight increase in surface polarity. At a higher loading of 0.5 wt.% $TiO_2$, the contact angle increased to 84º ± 2º, returning to a

value comparable to that of neat PLA. This behavior may be related to saturation effects or partial nanoparticle agglomeration, which can limit the influence of $TiO_2$ on surface chemistry.

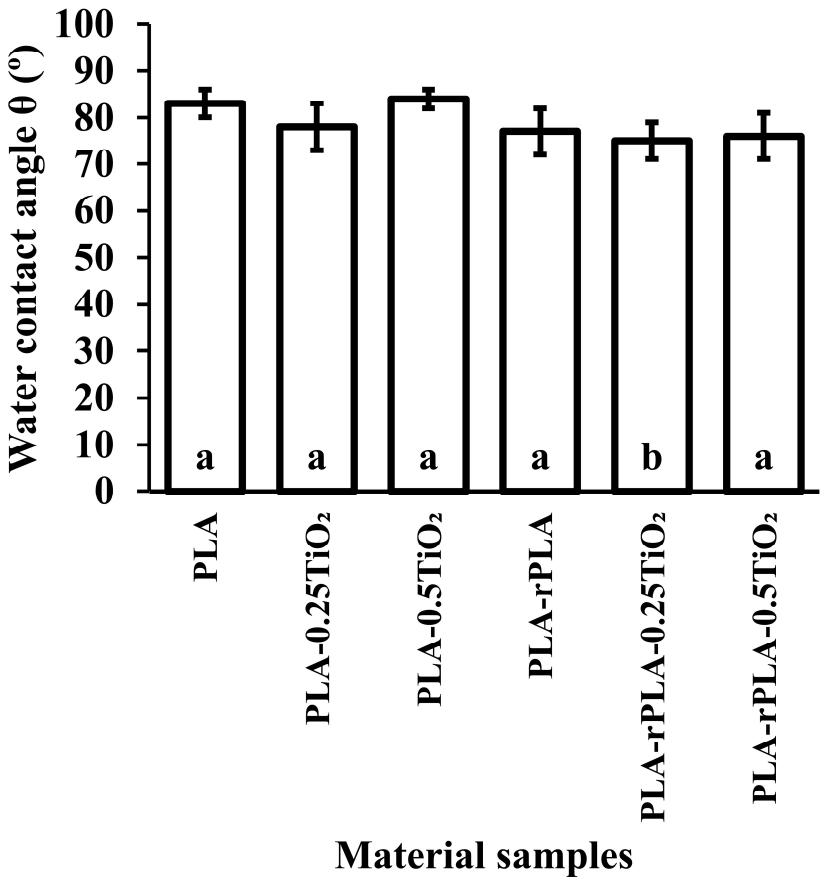


**Figure 10.** Water contact angle of PLA-based samples. Values with different letters are significantly different at $p < 0.05$.

**Table 4.** Water contact angle values of PLA-based parts.

| Material | Mean angle (º) |
|---|---|
| PLA | 83 ± 3 [a] |
| PLA-0.25$TiO_2$ | 78 ± 5 [a] |
| PLA-0.5$TiO_2$ | 84 ± 2 [a] |
| PLA-rPLA | 77 ± 5 [a] |
| PLA-rPLA-0.25$TiO_2$ | 75 ± 4 [b] |
| PLA-rPLA-0.5$TiO_2$ | 76 ± 5 [a] |

Values with different letters are significantly different at $p < 0.05$.

In PLA-rPLA blends, $TiO_2$ addition produced only minor variations in contact angle. PLA-rPLA-0.25$TiO_2$ and PLA-rPLA-0.5$TiO_2$ exhibited mean values of 75º ± 4º and 76º ± 5º, respectively, which are comparable to or slightly lower than that of the unfilled PLA-rPLA blend.

Although the mean values are relatively close, ANOVA results revealed statistically significant differences among formulations ($F = 3.99$, $p = 8.90 \times 10^{-3}$). Tukey's post hoc analysis indicates that PLA-rPLA-0.25$TiO_2$ forms a statistically distinct group with slightly lower contact angle values, suggesting a modest increase in surface hydrophilicity compared to the other formulations.

### *3.6. Disintegration under composting conditions*

The disintegration behavior of neat PLA, PLA-$TiO_2$ composites, PLA-rPLA blends, and PLA-rPLA-$TiO_2$ composites was investigated under controlled composting conditions over a 28-day period. The objective was to assess the influence of reprocessed content and $TiO_2$ incorporation on the environmental disintegrability of the materials, particularly in the context of end-of-life management strategies aligned with circular economy principles.

Visual observations in Figure 11 revealed a progressive disintegration of the samples throughout the test period. Neat PLA and PLA-rPLA 3D parts showed an increased opacity after only one day under composting, indicating that a water uptake process is taking place and/or the presence of a somewhat hydrolytic degradation process of the PLA-based polymeric matrix, which induces a change in the refraction index of the initial, mainly transparent, 3D parts. The change in the refraction index during the first day of the disintegration process was previously observed in PLA by Iglesias-Montes et al. [52] and rPLA systems by Arrieta et al. [53]. Then, PLA showed gradual surface erosion, while PLA-rPLA specimens exhibited faster fragmentation.

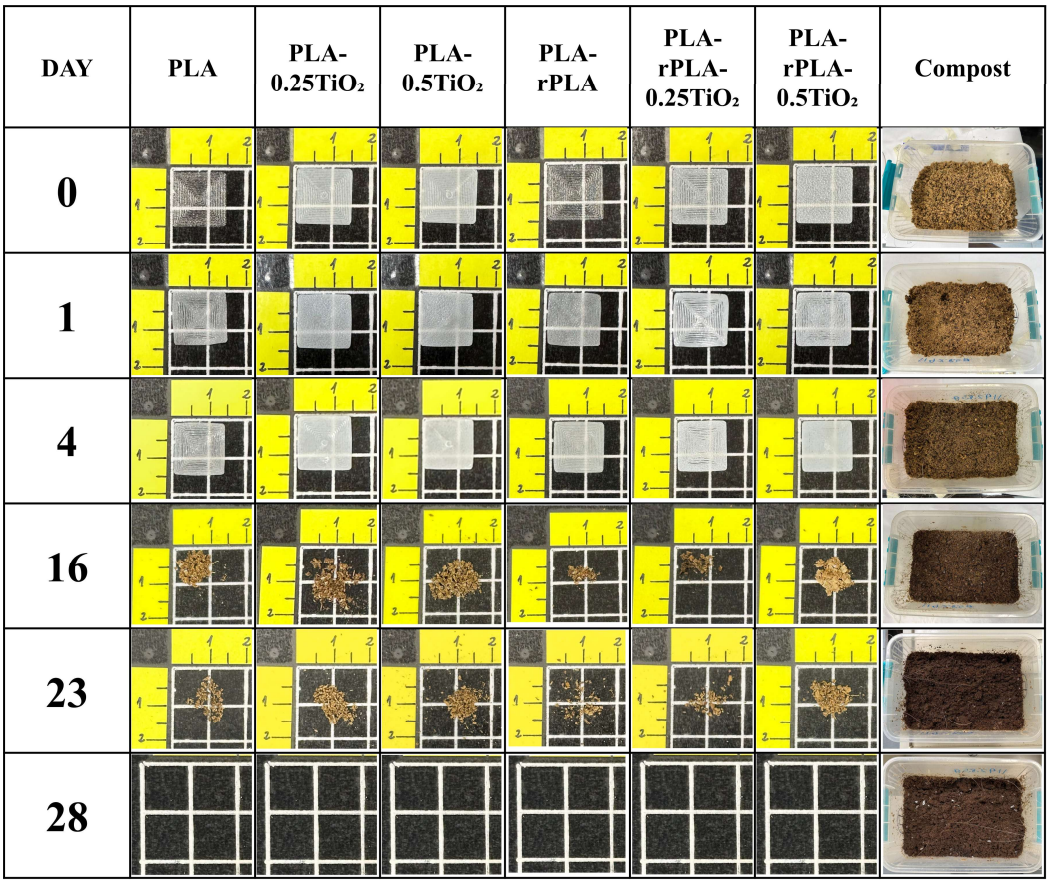


**Figure 11.** Visual degradation of PLA-based specimens during composting.

The addition of $TiO_2$ did not prevent visible disintegration but appeared to influence the rate and homogeneity of degradation, as composites retained structural integrity for slightly longer during the initial stages of composting. By the end of the test, all formulations had lost their physical form and were fully integrated into the compost matrix.

Mass loss profiles shown in Figure 12 provided quantitative evidence of the degradation kinetics. All materials followed a sigmoidal trend, with an initial lag phase during the first 5 days, followed by a rapid degradation stage between 10 and 20 days, and finally reaching near-complete mineralization (~90%–100%) in 28 days.

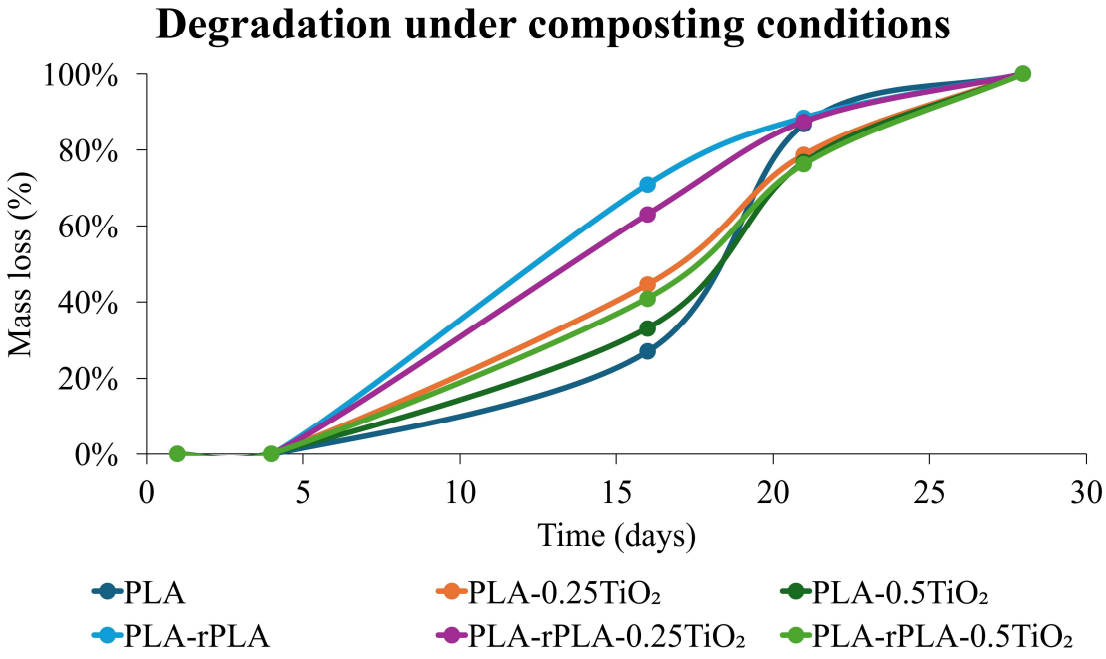


**Figure 12.** Mass loss during composting of PLA-based formulations.

Neat PLA reached ~95% mass loss, while PLA-rPLA achieved similar final values but with a faster onset of degradation, as mechanical reprocessing led to shorter polymer chains that further plasticize the polymeric matrix, being more susceptible to microorganisms' attack [25,54]. This mechanism is also consistent with the lower water contact angle observed in rPLA-containing formulations, which indicates increased surface polarity and improved water affinity, facilitating the hydrolysis process that precedes microbial assimilation [55–57]. The presence of $TiO_2$ slightly moderated degradation rates: PLA-$TiO_2$ composites showed a delayed transition into the rapid degradation stage compared to neat PLA. However, these effects were temporary, as final mass loss values converged among all systems. In PLA-rPLA-$TiO_2$ blends, the interaction between reprocessed content and nanoparticles balanced the kinetics. PLA-rPLA-0.25$TiO_2$ and PLA-rPLA-0.50$TiO_2$ degraded faster than neat PLA-$TiO_2$, but slower than PLA-rPLA without fillers.

Neat PLA and PLA with $TiO_2$ samples retained most of their structure up to day 16. However, PLA-rPLA blends, particularly the unfilled and 0.25 wt.% $TiO_2$ formulations, showed significant fragmentation after 16 days. By day 23, all specimens were heavily decomposed, with the rPLA-containing samples showing more advanced physical disintegration. This suggests that rPLA promotes a faster breakdown, possibly due to lower molecular weight and reduced crystallinity, which

enhance microbial accessibility. Additionally, specimens with higher $TiO_2$ content (0.50 wt.%) exhibited slightly more structural retention, which aligns with the known barrier properties of $TiO_2$, potentially slowing water uptake and hydrolysis. The quantitative results in Figure 12 show consistent trends. PLA-rPLA exhibited the highest degradation rate, reaching total mass loss by day 28. Neat PLA followed, with slightly lower mass loss than PLA-rPLA. Formulations containing $TiO_2$ showed a delayed degradation response, especially at 0.5 wt.%. Both PLA-$TiO_2$ and PLA-rPLA-$TiO_2$ samples degraded more slowly, particularly in the first 20 days. The presence of $TiO_2$ appears to inhibit the early stages of the hydrolysis process and microbial attack, likely due to its barrier and UV-shielding effects, as also reported in previous studies [4,6,21,23]. Interestingly, by day 28, all formulations achieved similar final mass loss values, indicating that $TiO_2$ delays but does not prevent complete degradation under composting conditions.

The accelerated degradation observed in PLA-rPLA systems is primarily associated with the reduction in molecular weight caused by thermo-mechanical degradation during reprocessing. These interpretations are inferred from macroscopic property trends and supported by literature reports rather than by direct microstructural observations. Multiple extrusion cycles induce chain scission in PLA, generating shorter polymer chains and increasing the concentration of terminal functional groups such as hydroxyl and carboxyl groups [24,25,55]. These structural modifications enhance the susceptibility of the polymer matrix to hydrolytic degradation, which constitutes the first stage of PLA biodegradation under composting conditions [55,57]. Shorter chains require less energy to undergo hydrolytic cleavage and, once fragmented, can diffuse more readily into the surrounding composting medium. Consequently, formulations containing rPLA typically exhibit faster mass loss and earlier fragmentation compared with neat PLA systems. Molecular weight reduction also affects the internal morphology of the material by altering the balance between amorphous and crystalline regions. Hydrolytic degradation occurs preferentially in amorphous domains, where molecular chains are less tightly packed and therefore more accessible to water molecules, while crystalline regions act as physical barriers that slow water diffusion and microbial attack [42,57]. The incorporation of rPLA can modify crystallization behavior during melt processing, often increasing the relative proportion or accessibility of amorphous regions, which further contributes to the accelerated degradation behavior observed in PLA-rPLA blends.

Surface wettability also influences the hydrolytic degradation of PLA-based materials. Increased surface polarity promotes water adsorption and diffusion into the polymer matrix, accelerating ester bond hydrolysis and initiating biodegradation [35,57]. Materials exhibiting lower water contact angles generally degrade more rapidly under composting conditions due to enhanced water–polymer interactions. Accordingly, the reduced contact angles observed in rPLA-containing formulations support the faster degradation rates measured during composting experiments.

The combined results obtained from thermal, mechanical, and biodegradation analyses suggest a consistent mechanistic relationship between the structural state of the polymer matrix and the observed material performance. In particular, the behavior of the PLA-rPLA systems can be interpreted as a consequence of molecular weight reduction induced by thermo-mechanical degradation during reprocessing.

The decrease in thermal stability observed in the TGA analysis for PLA-rPLA formulations indicates that chain scission occurs during the reprocessing step, leading to shorter polymer chains. These shorter chains reduce the energy required for thermal degradation and therefore lower the onset degradation temperature [24,25]. At the same time, molecular weight reduction affects the mechanical

response of the material by decreasing chain entanglement density and limiting plastic deformation mechanisms, which explains the reduced elongation at break observed in rPLA-containing samples.

These structural changes also influence the biodegradation behavior of the materials. Lower molecular weight chains and increased amorphous regions facilitate water diffusion into the polymer matrix, promoting hydrolytic degradation, which is the first stage of PLA biodegradation under composting conditions [42,55,57]. Consequently, the rPLA-containing systems show faster mass loss and earlier fragmentation during composting experiments.

The addition of $TiO_2$ nanoparticles partially counteracts some of these effects by introducing a rigid inorganic phase within the polymer matrix. The nanoparticles restrict polymer chain mobility and act as physical barriers to heat transfer and volatile diffusion, contributing to the improved thermal stability and increased stiffness observed in the nanocomposites [4,11,18]. However, due to the very low concentrations used in this study, the nanoparticles do not significantly alter the overall biodegradation behavior, indicating that the dominant factor controlling compostability remains the molecular structure of the PLA matrix. These results highlight the complex interplay between polymer degradation state, nanoparticle reinforcement, and environmental degradation mechanisms in PLA-based nanocomposites processed by FFF.

### *3.7. Statistical analysis*

Statistical analysis was conducted to determine whether the observed differences among formulations were significant. Table 5 summarizes the ANOVA results for Young's modulus, tensile strength, elongation at break, and water contact angle.

**Table 5.** One-way ANOVA results for mechanical and surface properties.

| Property | F | p-value | $\eta^2$ | Cohen's f |
|---|---|---|---|---|
| Young's modulus | 20.81 | $1.58 \times 10^{-1}$ | 0.658 | 1.388 |
| Tensile strength | 6.50 | $8.52 \times 10^{-5}$ | 0.376 | 0.776 |
| Elongation at break | 37.70 | $1.92 \times 10^{-16}$ | 0.777 | 1.868 |
| Water contact angle | 3.99 | $8.90 \times 10^{-3}$ | 0.454 | 0.912 |

The analysis revealed statistically significant differences among the formulations for all evaluated properties. Beyond statistical significance, effect size analysis was performed to evaluate the magnitude of the influence of formulation variables on the evaluated properties. The $\eta^2$ values ranged from 0.376 to 0.777, indicating that a substantial proportion of the observed variance in mechanical and surface properties can be attributed to differences in material formulation. In particular, elongation at break exhibited the largest effect size ($\eta^2 = 0.777$), suggesting that ductility is the property most strongly influenced by the incorporation of rPLA and $TiO_2$ nanoparticles. Young's modulus also showed a very large effect size ($\eta^2 = 0.658$), confirming that stiffness is highly sensitive to nanoparticle reinforcement and the presence of reprocessed material. Tensile strength presented a moderate-to-large effect ($\eta^2 = 0.376$), indicating that although differences exist among formulations, the load-bearing capacity of the material remains relatively stable across compositions. Finally, water contact angle displayed a moderate effect size ($\eta^2 = 0.454$), suggesting that surface wettability is influenced by formulation but to a lesser extent than the bulk mechanical properties. The corresponding Cohen's f

values (0.776–1.868) further confirm that the formulation variables produce large to very large effects, according to conventional interpretation thresholds.

The results demonstrate that even ultra-low $TiO_2$ concentrations can produce measurable changes in the thermal and mechanical response of PLA-based systems. This finding is particularly relevant because many previous studies rely on significantly higher nanoparticle contents to achieve similar improvements [4,18,47]. The present results suggest that relatively small amounts of $TiO_2$ may already influence chain mobility, crystallization behavior, and degradation kinetics, highlighting the efficiency of nanoparticle reinforcement at low loadings when dispersion is adequately achieved during melt processing [18]. This behavior also indicates that optimizing nanoparticle dispersion may be more critical than simply increasing filler concentration, especially in additive manufacturing materials where processability and filament quality are essential.

## 4. Conclusions

PLA-based composite filaments combining virgin PLA, 30 wt.% rPLA, and low $TiO_2$ loadings (0.25 and 0.50 wt.%) were successfully produced and subsequently transformed into 3D-printed specimens. The filaments and printed parts exhibited homogeneous morphology, with no visible phase separation at the studied $TiO_2$ concentrations.

FTIR results demonstrate that all formulations retain the characteristic chemical signature of PLA. The incorporation of rPLA and low $TiO_2$ loadings (0.25–0.5 wt.%) does not lead to the formation of new functional groups or measurable chemical interactions detectable by FTIR. Therefore, the observed differences in thermal, mechanical, and degradation behavior discussed could be attributed to physical effects, such as filler dispersion, interfacial interactions, and molecular weight variations, rather than to changes in the chemical structure of the polymer.

Thermogravimetric analysis results demonstrate that rPLA slightly reduces thermal stability due to prior degradation, while low concentrations of $TiO_2$ nanoparticles effectively delay thermal decomposition. This stabilizing effect is attributed to the barrier and heat-dissipation mechanisms of $TiO_2$, which hinder the diffusion of volatile degradation products and slow down the degradation process. These findings confirm that $TiO_2$ can enhance the thermal resistance of PLA-based composites, even in the presence of reprocessed content.

Tensile testing results demonstrate that low $TiO_2$ loadings effectively increase stiffness while preserving tensile strength in both virgin and rPLA systems. Although ductility is reduced compared to neat PLA, the PLA-rPLA-$TiO_2$ composites maintain balanced mechanical performance, making them suitable for additive manufacturing applications where rigidity and dimensional stability are prioritized.

Water contact angle measurements and composting tests revealed a relation between hydrophilicity and degradation behavior. The incorporation of rPLA increased surface polarity, reducing the water contact angle and accelerating biodegradation under composting conditions. The observed trends suggest that changes in biodegradation behavior are primarily driven by the presence of rPLA rather than by $TiO_2$-induced modifications of surface hydrophilicity.

The combined thermal, mechanical, and composting results suggest that the observed property changes are governed by the interplay between molecular weight reduction caused by PLA reprocessing and the reinforcing effect of $TiO_2$ nanoparticles acting as rigid inclusions within the polymer matrix.

Importantly, the results demonstrate that measurable reinforcement effects can be achieved using ultra-low $TiO_2$ concentrations, suggesting that optimized nanoparticle dispersion may represent a more efficient strategy than increasing filler loading in PLA-based additive manufacturing materials. The results also suggest the existence of an optimal nanoparticle concentration, where improved dispersion maximizes the stabilizing effect of $TiO_2$ without introducing aggregation-related defects. In the present study, this optimal range appears around 0.25 wt.% $TiO_2$ under the selected processing conditions.

Overall, at low concentrations (0.25–0.50 wt.%), $TiO_2$ nanoparticles increased the thermal stability and stiffness of PLA-based composites while preserving chemical integrity and maintaining compostability. The incorporation of rPLA ensured sustainability by closing material loops, while $TiO_2$ provided functional reinforcement to extend performance during use. The combined system, therefore, offers a viable route toward the development of eco-efficient filaments for additive manufacturing, particularly in applications where mechanical stability and controlled degradation are required. Operating within this low nanoparticle concentration range also allows the evaluation of reinforcement mechanisms without the need for compatibilizers or surface-modified nanoparticles, thereby maintaining a simple, scalable processing approach compatible with FFF technologies.

Future work will focus on detailed microstructural characterization by SEM to assess $TiO_2$ dispersion and interfacial quality, DSC analysis to quantify thermal transitions and crystallinity, rheological testing to relate melt behavior to extrusion and printing performance, and molecular weight determination through techniques such as gel permeation chromatography (GPC) to evaluate the effects of reprocessing and nanoparticle incorporation on polymer chain integrity. Additional studies will include ultraviolet–visible spectroscopy (UV-Vis) to evaluate UV-shielding capability and post-aging experiments to assess long-term property retention through combined mechanical, thermal, and microstructural analyses.

## Use of AI tools declaration

The authors declare AI-assisted tools were used solely to enhance grammar, spelling, and readability. No AI tool was used for data generation, analysis, or interpretation. All intellectual and scientific contributions are the authors' original work.

## Acknowledgments

The authors thank the I+D+i PID2024-157368NB-C32 project by MCIN/AEI/10.13039/501100011033 "FEDER a way of making Europe"; Secretaria Nacional de Ciencia, Tecnología e Innovación (SENACYT) from Panama, grant number DDCCT—No 142-2023 for the financial support provided through the MCIM-AZUERO-2023-005 scholarship and the research project APY-SIES-2025A-32, grant number DDCCT—No 057-2025. Simón Faba acknowledges financial support from the National Agency for Research and Development (ANID-Chile) through the Postdoctoral Fellowship for Research Abroad (Grant No. 74230053).

## Author contributions

Thomas Rodríguez: conceptualization; methodology; investigation; writing—original draft. Nacarí Marín-Calvo: writing—review & editing; visualization; funding acquisition. Yessica Sáez:

writing—review & editing; visualization. Simón Faba: writing—review & editing; investigation. Marina Patricia Arrieta: writing—review & editing; investigation. Edwin Collado: writing—review & editing; formal analysis; supervision.

## Conflict of interest

The authors declare no conflict of interest.

## References


1. Kaseem M, Hamad K, Rehman ZU (2019) Review of recent advances in polylactic acid/$TiO_2$ composites. *Materials* 12: 3659. https://doi.org/10.3390/ma12223659
2. Rafiee M, Abidnejad R, Ranta A, et al. (2021) Exploring the possibilities of FDM filaments comprising natural fiber-reinforced biocomposites for additive manufacturing. *AIMS Mater Sci* 8: 524–537. https://doi.org/10.3934/matersci.2021032
3. Saeed U (2020) Wood cellulose fibers reinforced polylactic acid composite: Mechanical, thermomechanical characteristics and orientation of fiber. *AIMS Mater Sci* 7: 9–23. https://doi.org/10.3934/matersci.2020.1.9
4. Bikiaris ND, Koumentakou I, Samiotaki C, et al. (2023) Recent advances in the investigation of poly(lactic acid) (PLA) nanocomposites: Incorporation of various nanofillers and their properties and applications. *Polymers* 15: 1196. https://doi.org/10.3390/polym15051196
5. Antunes A, Popelka A, Aljarod O, et al. (2020) Effects of rutile-$TiO_2$ nanoparticles on accelerated weathering degradation of poly(lactic acid). *Polymers* 12: 1096. https://doi.org/10.3390/polym12051096
6. Cao Y, Xu P, Lv P, et al. (2020) Excellent UV resistance of polylactide by interfacial stereocomplexation with double-shell-structured $TiO_2$ nanohybrids. *ACS Appl Mater Interfaces* 12: 49090–49100. https://doi.org/10.1021/acsami.0c14423
7. Kechagias JD (2022) Materials for additive manufacturing. *AIMS Mater Sci* 9: 785–790. https://doi.org/10.3934/matersci.2022048
8. Ramírez-Prieto JS, Martínez-Yáñez JS, González-Hernández AG (2025) Effect of raster angle on the tensile and flexural strength of 3D printed PLA + parts. *AIMS Mater Sci* 12: 363–379. https://doi.org/10.3934/matersci.2025019
9. Sepúlveda-Carter J, Faba S, Sánchez Rodríguez M, et al. (2025) Reprocessing of simulated industrial PLA waste for food contact applications. *Polymers* 17: 2439. https://doi.org/10.3390/polym17182439
10. Bergaliyeva S, Sales DL, Jiménez Cabello JM, et al. (2023) Thermal and mechanical properties of reprocessed polylactide/titanium dioxide nanocomposites for material extrusion additive manufacturing. *Polymers* 15: 3458. https://doi.org/10.3390/polym15163458
11. Zhang H, Huang J, Yang L, et al. (2015) Preparation, characterization and properties of PLA/$TiO_2$ nanocomposites based on a novel vane extruder. *RSC Adv* 5: 4639–4647. https://doi.org/10.1039/C4RA14538K
12. Zhu Y, Buonocore GG, Lavorgna M, et al. (2011) Poly(lactic acid)/titanium dioxide nanocomposite films: Influence of processing procedure on dispersion of titanium dioxide and photocatalytic activity. *Polym Compos* 32: 519–528. https://doi.org/10.1002/pc.21068

13. Li S, Chen G, Qiang S, et al. (2020) Synthesis and evaluation of highly dispersible and efficient photocatalytic $TiO_2$/poly lactic acid nanocomposite films via sol-gel and casting processes. *Int J Food Microbiol* 331: 108763. https://doi.org/10.1016/j.ijfoodmicro.2020.108763
14. Zorah M, Mustapa IR, Daud N, et al. (2020) Improvement thermomechanical properties of polylactic acid via titania nanofillers reinforcement. *J Adv Res Fluid Mech Therm Sci* 70: 97–111. https://doi.org/10.37934/arfmts.70.1.97111
15. Shebi A, Lisa S (2019) Evaluation of biocompatibility and bactericidal activity of hierarchically porous PLA-$TiO_2$ nanocomposite films fabricated by breath-figure method. *Mater Chem Phys* 230: 308–318. https://doi.org/10.1016/j.matchemphys.2019.03.045
16. Karagiannis E, Papadaki D, Assimakopoulos MN (2022) Circular self-cleaning building materials and fabrics using dual doped $TiO_2$ nanomaterials. *AIMS Mater Sci* 9: 534–553. https://doi.org/10.3934/matersci.2022032
17. Irhayyim SS, Hammood HS, Abdulhadi HA (2019) Effect of nano-$TiO_2$ particles on mechanical performance of Al–CNT matrix composite. *AIMS Mater Sci* 6: 1124–1134. https://doi.org/10.3934/matersci.2019.6.1124
18. Athanasoulia IGI, Tarantili PA (2019) Thermal transitions and stability of melt mixed $TiO_2$/poly(L-lactic acid) nanocomposites. *Polym Eng Sci* 59: 704–713. https://doi.org/10.1002/pen.24986
19. Nakayama N, Hayashi T (2007) Preparation and characterization of poly(L-lactic acid)/$TiO_2$ nanoparticle nanocomposite films with high transparency and efficient photodegradability. *Polym Degrad Stab* 92: 1255–1264. https://doi.org/10.1016/j.polymdegradstab.2007.03.026
20. Baek N, Kim YT, Marcy JE, et al. (2018) Physical properties of nanocomposite polylactic acid films prepared with oleic acid modified titanium dioxide. *Food Packag Shelf Life* 17: 30–38. https://doi.org/10.1016/j.fpsl.2018.05.004
21. Segura González EA, Olmos D, Lorente MÁ, et al. (2018) Preparation and characterization of polymer composite materials based on PLA/$TiO_2$ for antibacterial packaging. *Polymers* 10: 1365. https://doi.org/10.3390/polym10121365
22. Buzarovska A, Dinescu S, Chitoiu L, et al. (2018) Porous poly(L-lactic acid) nanocomposite scaffolds with functionalized $TiO_2$ nanoparticles: properties, cytocompatibility and drug release capability. *J Mater Sci* 53: 11151–11166. https://doi.org/10.1007/s10853-018-2415-0
23. Feng S, Zhang F, Ahmed S, et al. (2019) Physico-mechanical and antibacterial properties of PLA/$TiO_2$ composite materials synthesized via electrospinning and solution casting processes. *Coatings* 9: 525. https://doi.org/10.3390/coatings9080525
24. Velghe I, Buffel B, Vandeginste V, et al. (2023) Review on the degradation of poly(lactic acid) during melt processing. *Polymers* 15: 2047. https://doi.org/10.3390/polym15092047
25. Badia JD, Ribes-Greus A (2016) Mechanical recycling of polylactide, upgrading trends and combination of valorization techniques. *Eur Polym J* 84: 22–39. https://doi.org/10.1016/j.eurpolymj.2016.09.005
26. Comisión Europea (2025) Estrategia sobre plásticos. Accessed May 31 2025. Available from: https://environment.ec.europa.eu/strategy/plastics-strategy_en.
27. Comisión Europea (2018) Una estrategia europea para el plástico en una economía circular. Accessed May 31 2025. Available from: https://eur-lex.europa.eu/legal-content/ES/TXT/?uri=CELEX:52018DC0028.

28. Parlamento Europeo y Consejo de la Unión Europea (2019) Directiva (UE) 2019/904 relativa a la reducción del impacto de determinados productos de plástico en el medio ambiente. Accessed May 31 2025. Available from: https://www.boe.es/buscar/doc.php?id=DOUE-L-2019-81016.
29. NatureWorks LLC (2025) Ingeo™ biopolymer 2003D technical data sheet for fresh food packaging and food serviceware. Accessed Oct 14 2025. Available from: https://www.natureworksllc.com/technologies-and-products/products/2-series-for-extrusion-thermoforming.
30. Sigma-Aldrich (2025) Titanium dioxide. Accessed Oct 14 2025. Available from: https://www.sigmaaldrich.com/US/en/product/sigald/14021.
31. Kosowska K, Szatkowski P (2020) Influence of ZnO, $SiO_2$ and $TiO_2$ on the aging process of PLA fibers produced by electrospinning method. *J Therm Anal Calorim* 140: 1769–1778. https://doi.org/10.1007/s10973-019-08890-6
32. ASTM International (2021) ASTM E1252-98(2021): Standard practice for general techniques for obtaining infrared spectra for qualitative analysis. https://doi.org/10.1520/E1252-98R21
33. ISO (2019) ISO 527-1:2019 plastics—Determination of tensile properties—Part 1: General principles. International Organization for Standardization. Available from: https://www.iso.org/standard/527-1.
34. UNE (2016) UNE-EN ISO 20200:2016 plásticos. Determinación del grado de desintegración de materiales plásticos bajo condiciones de compostaje simuladas en un ensayo a escala de laboratorio. Accessed Apr 28 2025. Available from: https://www.en-standard.eu/une-en-iso-20200-2016-plastics-determination-of-the-degree-of-disintegration-of-plastic-materials-under-simulated-composting-conditions-in-a-laboratory-scale-test-iso-20200-2015/.
35. Arrieta MP, López J, Rayón E, et al. (2014) Disintegrability under composting conditions of plasticized PLA–PHB blends. *Polym Degrad Stab* 108: 307–318. https://doi.org/10.1016/j.polymdegradstab.2014.01.034
36. UNE (2013) UNE-EN 828:2013 adhesivos. Mojabilidad. Determinación por medición del ángulo de contacto y de la energía libre superficial de una superficie sólida. Accessed Apr 28 2025. Available from: https://www.une.org/encuentra-tu-norma/busca-tu-norma/norma?c=N0051185.
37. Zhao Y, Chen Y, Zhou Y (2019) Novel mechanical models of tensile strength and elastic property of FDM AM PLA materials: Experimental and theoretical analyses. *Mater Des* 181: 108089. https://doi.org/10.1016/j.matdes.2019.108089
38. Carrasco F, Pagès P, Gámez-Pérez J, et al. (2010) Processing of poly(lactic acid): Characterization of chemical structure, thermal stability and mechanical properties. *Polym Degrad Stab* 95: 116–125. https://doi.org/10.1016/j.polymdegradstab.2009.11.045
39. Kister G, Cassanas G, Vert M (1998) Effects of morphology, conformation and configuration on the IR and Raman spectra of various poly(lactic acid)s. *Polymer* 39: 267–273. https://doi.org/10.1016/S0032-3861(97)00229-2
40. Buzarovska A, Grozdanov A (2012) Biodegradable poly(L-lactic acid)/$TiO_2$ nanocomposites: thermal properties and degradation. *J Appl Polym Sci* 123: 2187–2193. https://doi.org/10.1002/app.34729
41. Jakić M, Perinović Jozić S, Santro A, et al. (2024) Thermal analysis of the biodegradable polymer PVA/PEO blends. *Teh Glas* 18: 224–228. https://doi.org/10.31803/TG-20231008184941

42. Farah S, Anderson DG, Langer R (2016) Physical and mechanical properties of PLA, and their functions in widespread applications—A comprehensive review. *Adv Drug Deliv Rev* 107: 367–392. https://doi.org/10.1016/j.addr.2016.06.012
43. Tymrak BM, Kreiger M, Pearce JM (2014) Mechanical properties of components fabricated with open-source 3-D printers under realistic environmental conditions. *Mater Des* 58: 242–246. https://doi.org/10.1016/j.matdes.2014.02.038
44. Makalesi A, Özsoy K, Erçetin A, et al. (2021) Comparison of mechanical properties of PLA and ABS based structures produced by fused deposition modelling additive manufacturing. *Eur J Sci Technol* 27: 802–809. https://doi.org/10.31590/EJOSAT.983317
45. İncesu R, Akderya T (2024) The influence of printing speed and temperature on the mechanical, absorptive, and morphological properties of PLA-based hybrid materials produced with an FDM-type 3D printer. *Polymers* 16: 2771. https://doi.org/10.3390/polym16192771
46. Maldonado A, Aguilar T, Hauser C, et al. (2024) Ethylene scavenging films based on ecofriendly plastic materials and nano-$TiO_2$: Preparation, characterization, and in vivo evaluation. *Polymers* 16: 853. https://doi.org/10.3390/polym16060853
47. Sinha Ray S, Okamoto M (2003) Polymer/layered silicate nanocomposites: A review from preparation to processing. *Prog Polym Sci* 28: 1539–1641. https://doi.org/10.1016/j.progpolymsci.2003.08.002
48. Yang J, Bei J, Wang S (2002) Enhanced cell affinity of poly(D,L-lactide) by combining plasma treatment with collagen anchorage. *Biomaterials* 23: 2607–2614. https://doi.org/10.1016/S0142-9612(01)00400-8
49. Luque-Agudo V, Gallardo-Moreno AM, González-Martín ML (2021) Influence of solvent and substrate on hydrophobicity of PLA films. *Polymers* 13: 4289. https://doi.org/10.3390/polym13244289
50. Cai K, Yao K, Lin S, et al. (2002) Poly(D,L-lactic acid) surfaces modified by silk fibroin: Effects on the culture of osteoblast in vitro. *Biomaterials* 23: 1153–1160. https://doi.org/10.1016/S0142-9612(01)00230-7
51. Zenkiewicz M, Richert J, Rytlewski P, et al. (2009) Characterisation of multi-extruded poly(lactic acid). *Polym Test* 28: 412–418. https://doi.org/10.1016/j.polymertesting.2009.01.012
52. Iglesias-Montes ML, Luzi F, Dominici F, et al. (2021) Migration and degradation in composting environment of active polylactic acid bilayer nanocomposites films: Combined role of umbelliferone, lignin and cellulose nanostructures. *Polymers* 13: 282. https://doi.org/10.3390/polym13020282
53. Arrieta MP, Beltrán FR, Abarca de las Muelas SS, et al. (2022) Development of tri-layer antioxidant packaging systems based on recycled PLA/sodium caseinate/recycled PLA reinforced with lignocellulosic nanoparticles extracted from yerba mate waste. *Express Polym Lett* 16: 881–900. https://doi.org/10.3144/expresspolymlett.2022.64
54. Beltrán FR, Arrieta MP, Elena Antón D, et al. (2021) Effect of yerba mate and silk fibroin nanoparticles on the migration properties in ethanolic food simulants and composting disintegrability of recycled PLA nanocomposites. *Polymers* 13: 1925. https://doi.org/10.3390/polym13121925
55. Jamshidian M, Tehrany EA, Imran M, et al. (2010) Poly-lactic acid: Production, applications, nanocomposites, and release studies. *Compr Rev Food Sci Food Saf* 9: 552–571. https://doi.org/10.1111/j.1541-4337.2010.00126.x

56. Limsukon W, Rubino M, Rabnawaz M, et al. (2023) Hydrolytic degradation of poly(lactic acid): Unraveling correlations between temperature and the three phase structures. *Polym Degrad Stab* 217: 110537. https://doi.org/10.1016/j.polymdegradstab.2023.110537
57. Luo Y, Lin Z, Guo G (2019) Biodegradation assessment of poly(lactic acid) filled with functionalized titania nanoparticles (PLA/$TiO_2$) under compost conditions. *Nanoscale Res Lett* 14: 56. https://doi.org/10.1186/s11671-019-2891-4


AIMS Press